EEGG: An Analytic Brain-Computer Interface Algorithm

Gang Liu, *Student Member, IEEE*, and Jing Wang

***Abstract*— *Objective.* Modeling the brain as a white box is vital for investigating the brain. However, the physical properties of the human brain are unclear. Therefore, BCI algorithms using EEG signals are generally a data-driven approach and generate a black- or gray-box model. This paper presents the first EEG-based BCI algorithm (EEG-BCI using Gang neurons, EEGG) decomposing the brain into some simple components with physical meaning and integrating recognition and analysis of brain activity. *Approach.* Independent and interactive components of neurons or brain regions can fully describe the brain. This paper constructed a relation frame based on the independent and interactive compositions for intention recognition and analysis using a novel dendrite module of Gang neurons. A total of 4,906 EEG data of left- and right-hand motor imagery (MI) from 26 subjects were obtained from GigaDB. Firstly, this paper explored EEGG's classification performance by cross-subject accuracy. Secondly, this paper transformed the trained EEGG model into a relation spectrum expressing independent and interactive components of brain regions. Then, the relation spectrum was verified using the known ERD/ERS phenomenon. Finally, this paper explored the previously unreachable further BCI-based analysis of the brain. *Main results.* (1) EEGG was more robust than typical "CSP+" algorithms for the low-quality data. (2) The relation spectrum showed the known ERD/ERS phenomenon. (3) Interestingly, EEGG showed that interactive components between brain regions suppressed ERD/ERS effects on classification. This means that generating fine hand intention needs more centralized activation in the brain. *Significance.* EEGG decomposed the biological EEG-intention system of this paper into the relation spectrum inheriting the Taylor series (*in analogy with the data-driven but human-readable Fourier transform and frequency spectrum*), which offers a novel frame for analysis of the brain.**

***Index Terms*— Brain-computer interface, Gang neuron, white box, EEG, signal processing, system identification, analysis.**

I. Introduction

BRAIN-COMPUTER interface (BCI) based on electroencephalogram (EEG) is a technology that translates EEG signals recording a user's brain activity into control commands [1]–[4]. The model of the biological EEG-intention system is at the heart of BCI technology. Classically, the modeling approaches can be classified into the physics-based white-box approach, data-driven black-box approach, and physics- and data-driven gray-box approach [5], [6]. Biologists and clinicians prefer the white-box models because they are easy to understand and can be used to analyze biological mechanisms [7]. However, most of the existing EEG-based BCIs are data-driven because specific physical properties of intention are still a mystery. Restricted by data-driven basic machine learning (ML) algorithms(e.g., Support Vector Machines (SVM) [8], Neural Network (NN), and Bayesian Classifier [9]), traditional EEG-based BCIs usually model the biological EEG-intention system as a black box [8], [10].

In recent years, studies on the interpretability of ML outputs(e.g., feature visualization for deep networks [11], attribution for convolutional networks [12], and dimensionality reduction [13]) have been emerging in computer vision and natural language processing. Moreover, interpretable approaches have been used to explain the BCI model's outputs [14]. For instance, Layerwise relevance propagation (LRP) explains individual deep network decisions/outputs in the literature [14]. However, it is necessary to clarify that "Interpretation" refers to roughly explaining the outputs of the black-box model (e.g., deep neural networks) rather than reading the model's parameters [14]. Therefore, it only conforms to the definition of gray-box [6].

One of the most significant challenges of science today is to unlock the mysteries of the brain (i.e., the biological EEG-intention system) [15]. Nevertheless, the black- or gray-box model cannot resolve the brain's specific properties, and modeling the brain as a traditional white-box model requires known specific brain properties. Therefore, the brain's specific properties and traditional white-box model are prerequisites for each other, which is an endless loop. Fortunately, the key of the white-box model is essentially to give each model parameter a physical meaning, and the modeling approach based on physical properties is one of the ways, but not the only one, to assign the physical meaning to the parameters.

- **Introduction of Scheme (see Fig. 1)**

Fourier transform in signal processing has proved that decomposing an unknown composition into some simple components with physical meaning can effectively tackle this kind of complicated problem [19]. Therefore, learning from the ideas of Fourier transform, as long as the EEG-intent system is decomposed into parameters with physical meaning, the data-driven model is also a human-readable white-box model.

Manuscript received August 10, 2021; revised October 30, 2021, December 24, 2021, and January 18, 2022; accepted February 4, 2022. Date of publication February 7, 2022; date of current version March 22, 2022. This work was supported by the Science and Technology Project of Shaanxi Province under Grant 2019SF-109. *(Corresponding author: Jing Wang.)*

The authors are with the iHarbour Academy of Frontier Equipment, Institute of Robotics and Intelligent Systems, Xi'an Jiaotong University, Shaanxi 710049, China (e-mail: gangliu.6677@gmail.com; wangpele@gmail.com).

Digital Object Identifier 10.1109/TNSRE.2022.3149654

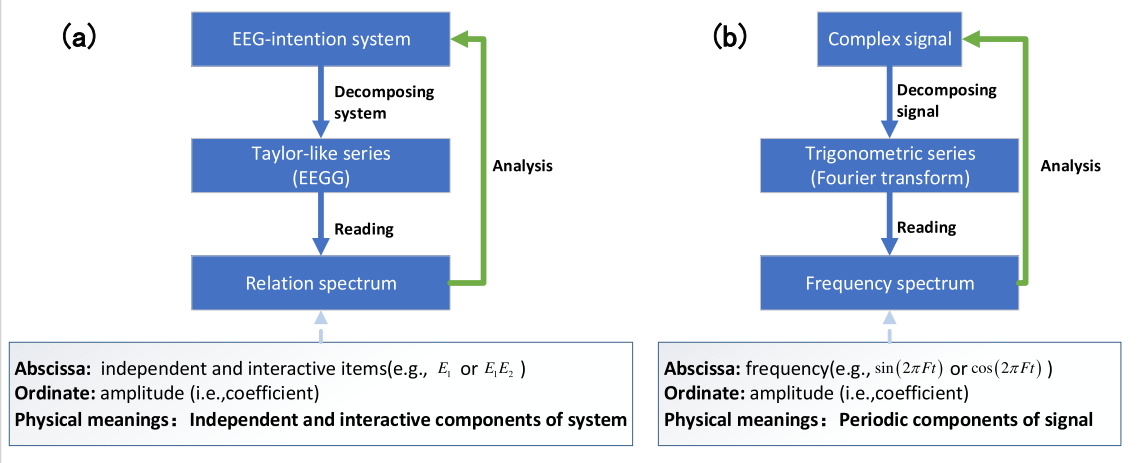

Fig. 1. Explanation of EEGG analysis analogous to Fourier analysis. (a) Explanation of EEGG analysis. (b)Explanation of Fourier analysis. In Fig. 1b, *F* represents the frequency, and *sin*(2π*Ft*) or *cos*(2π*Ft*) represent an example of the complete form of the abscissa. There are two famous function decomposition methods in math: the power series (e.g., Taylor series) and the trigonometric series (e.g., Fourier series) [16]. In mathematics, the Fourier series is the study of the way general functions may be represented or approximated by sums of simpler trigonometric functions [17], [18]. Fourier analysis is the latter (i.e., trigonometric series), and the theory used in this paper is the former. Fourier transform decomposes signal, and EEGG decomposes system. From a polynomial perspective, EEGG's process can be roughly understood as decomposing the biological EEG-intention system into thousands of polynomial terms (Multiple regression is the traditional method for solving polynomial terms. However, it cannot achieve thousands of polynomial terms due to the high computational complexity, yet EEGG completed the process. It is well known that terms of multiple regression can be used to analyze various systems; thus, EEGG can also be used for analysis).

In addition to the trigonometric series (Fourier transform), Taylor series also have physical meaning. For example, items of Taylor series contain E_1(first-order independent component), E_1^2(second-order independent component), and E_1E_2 (second-order interactive component), etc, where $E_1$and E_2 are independent variables. These components represent the effects of independent variables(model inputs) on the dependent variable(model output). In 2020, the researchers of this paper proposed a basic machine learning algorithm, Dendrite Net [20]. The central concept of Dendrite Net is that the algorithm can recognize the class after learning, if the output's logical expression contains the corresponding class's logical relation among inputs (and\or\not) [20]. Interestingly, the model using Dendrite Net can be translated into Relation Spectrum consisting of independent components and interactive components (Taylor-like series). However, its performance on the EEG-intent system is unknown.

Independent and interactive components of neurons or brain regions can fully describe the brain [21]. Therefore, the independent and interactive components are regarded as simple components with a physical meaning. This paper proposed a white-box relation frame (EEGG) based on brain regions' independent and interactive components using a residual dendrite module of Gang neuron (Residual Dendrite Net, ResDD, an improved Dendrite Net which is different from [20]). **The trained EEGG model not only can be used for online classification but can also be transformed into a relation spectrum expressing independent and interactive components of brain regions for offline analysis. This paper addresses the following major questions of this algorithm/frame.**

Q(1): This paper compared the classification performance between EEGG and other classic algorithms and further explored its advantages, disadvantages, and theoretical reasons for the performance.

Q(2): Since this paper decomposed the biological EEG-intention system into a relation spectrum (Taylor-like series) for the first time, the rationality of EEGG decomposition was verified by exploring whether the components in the relation spectrum contained the known ERD/ERS phenomenon.

Q(3): Based on the rationality of EEGG decomposition, this paper explored the previously unreachable further BCI-based analysis of the brain.

This paper is organized as follows. Section II introduces EEGG. Section III introduces experiments. Section IV presents the results. Section V discusses the results. Conclusions and outlook are given in Section VI. In addition, to make it easier to understand, some related concepts and theoretical backgrounds were clarified in TABLE I.

II. EEGG

A. Model Building for Classification

The architecture of the EEGG model for classification is shown in Fig. 2. It should be noted that the "Spatial filter" and "Power calculation" of EEGG refer to implementing the corresponding effects of previous single algorithms rather than using the corresponding single algorithms(e.g., CSP) [32]. Concretely, we constructed modules with corresponding functions. However, the preset parameters are not solved separately but are obtained by regarding the EEGG as a whole. EEGG model is an end-to-end model. The input of EEGG is the EEG signal after band-pass filtering, and there is no need for separate spatial filtering, feature extraction, or other processing. The independent and interactive components of brain regions are stored in weights $\boldsymbol{W}$. Weights are optimized by minimizing

TABLE I
CLARIFICATION OF CONCEPTS AND THEORETICAL BACKGROUNDS

Concepts	Clarification or explanation
Biological EEG-intention system	The human brain itself can be regarded as a system [22]. The biological EEG-intention system is a biological information transmission system that maps brain activities to certain intentions (or instructions to drive muscles). EEG records brain activities.
The quality of EEG data	The EEG signal is different from the traditional sensor signal (e.g., pressure sensor signal). In a specific paradigm, the quality of the EEG signal is affected by a variety of uncontrollable factors such as the subject's EEG intensity, the subject's attention, the subject's psychology [23]–[26]. Poor-quality data refers to the EEG data with less useful information about specific intentions. Good-quality data refers to the EEG data with more useful information about specific intentions. Therefore, it is difficult to calibrate the quality of EEG data for a specific paradigm.
Factors that affect model performance	There are only two factors that affect model performance: data and algorithm [27], [28]. One factor can be inferred by fixing another. Specifically, when building some models using the same data but different algorithms, we can infer the performance of the algorithms by the model performance. When building some models using the same algorithm but different data, we can infer the quality of data by the model performance.
Why EEGG is an end-to-end frame?	EEGG consists of the Spatial filter, Power calculation, and ResDD Neural Network(see Fig. 2). Traditionally, the preset parameters in the above three parts are calculated separately. Therefore, it is difficult to determine whether the parameters are optimal after combining these three parts. Parameter optimization using an end-to-end manner solves this problem. This step can be understood in analogy with the existing modeling methods. For instance, Model (1):the combination of wavelet transform (DWT) and multi-layer perceptron (MLP) [29]; Model (2) :convolutional neural network(CNN) [30]. The preset parameters in each part in Model (1) are solved separately; however, the preset parameters in Model (2) are solved in an end-to-end manner. Without an emphasis on the wavelet properties, the role of the convolutional layer in CNN is similar to DWT(convolution) [29], [30]. Yet, the values of the preset parameters in the convolutional layer are related to the subsequent fully connected layer(MLP).
Training data for machine learning [27], [28]	The training data is composed of samples, and each sample contains common information (which is useful for learning) and personalized information (e.g., noise and unique attributes of a single sample).
Machine learning for classification or regression (supervised) [20], [27], [28]	The goal of basic machine learning is to learn the mapping relation between the input space and the output space. **It is worth noting that the machine learning model should learn the common information in data as much as possible to ensure better generalization ability or robustness. Therefore, controlling the machine learning model's mapping ability or expression ability can make it learn as little personalized information as possible, thereby avoiding overfitting (that is, improving the generalization ability or robustness)**.
Central limit theorem (CLT) [31]	The central limit theorem establishes that, in many situations, when independent random variables are added, their properly normalized sum tends toward a normal distribution (informally a bell curve) even if the original variables themselves are not normally distributed. The normal distribution can be obeyed by default when the sample size is large, and the t-test can be used. Therefore, the t-test of relation items in this paper is feasible.

loss function using backpropagation (*Recommended optimizer: SGD in PyTorch*). The mean-square error (MSE) was the loss function used in this paper. In the rest of this section, we will introduce each step in detail.

1) Spatial Filter (see Fig.2a): Raw EEG scalp potentials are known to have poor spatial resolution due to volume conduction [33]. Therefore, spatial filters are extremely useful in the BCI model, especially MI-based BCI, to improve the signal-to-noise ratio [32].

Spatial filters aim to project the signal $\boldsymbol{E}^{\text{Input}}(t) \in \mathbb{R}^{NC}$ in the original sensor space to $\boldsymbol{E}^{\text{Spatial filtering}}(t) \in \mathbb{R}^{NC}$, which lives in the surrogate sensor space.

$$\boldsymbol{E}^{\text{Spatial filtering}}(t) = \left(\boldsymbol{E}^{\text{Input}}(t)\right)^{\mathrm{T}} \boldsymbol{W}_1 \tag{1}$$

where $\boldsymbol{W}_1 \in \mathbb{R}^{NC\times NC}$ is the weight matrix of the spatial filter, NC is the number of channels. A traditional spatial filter is a single algorithm (e.g., CSP, PCA, and ICA) [32], [34], [35]. The weight matrix $\boldsymbol{W}_1$ of the traditional spatial filter can be solved in two ways: an EEG-data-driven and unsupervised manner (e.g., PCA and ICA) [32] or a simple data-driven and supervised manner (e.g., CSP) [32]. However, both ways are not associated with later feature extraction and classification algorithms, which cannot ensure that the weight matrix $\boldsymbol{W}_1$ is optimal or suboptimal for later processing steps. Therefore, in the EEGG frame, the spatial filter solution is integrated into the end-to-end model. The weight matrix in the spatial filter is associated with the later power calculation and ResDD neural network.

2) Power Calculation (see Fig.2b): After spatial filtering, we calculate the power of each channel of $\boldsymbol{E}^{\text{Spatial filtering}}(t)$. Unlike the previous method, the unsigned characteristic of EEG signals in the record is taken into account. EEGG uses the variance or standard error instead of the magnitude squared to remove the direct current (DC) component [37]. Likewise, power calculation is also integrated into the end-to-end model rather than a single algorithm. The formulas are as follows.

$$P_i = \frac{\sum_{j=1}^{NL}\left(D_{ij} - \overline{D_i}\right)^2}{NL} \quad \text{or} \quad \sqrt{\frac{\sum_{j=1}^{NL}\left(D_{ij} - \overline{D_i}\right)^2}{NL}} \tag{2}$$

where $i \in [1, NC]$, $P_i \in \mathbb{R}$ is the power of the $i-$ th channel, $D_{ij} \in \mathbb{R}^{NC\times NL}$ expresses the $j-$th data point of the $i-$th channel. NC is the number of channels. After the power calculation step, a $1 \times NC$ vector is obtained.

3) ResDD Neural Network (see Fig.2c): A traditional artificial neuron was expressed as $f(wx + b)$ or $f(\boldsymbol{W}X)$ where $w, b, x, \boldsymbol{W}$, and $\boldsymbol{X}$ expressed the weight, bias, inputs, weight matrix, and input vector with element 1, respectively. f was activation function. This artificial neuron was designed by the stereotypical knowledge of biological neurons 70 years ago, and the design did not consider dendrites' information processing capacity. In 2020, Albert Gidon *et al.* demonstrated that biological dendrites participate in the pre-calculation of input data [38]. Subsequently, a Gang neuron was presented [36]. ResDD is one of the dendrite modules in Gang neurons. Previously, Dendrite Net was proposed, and its nonlinear mapping, generalization capability, and identification capability

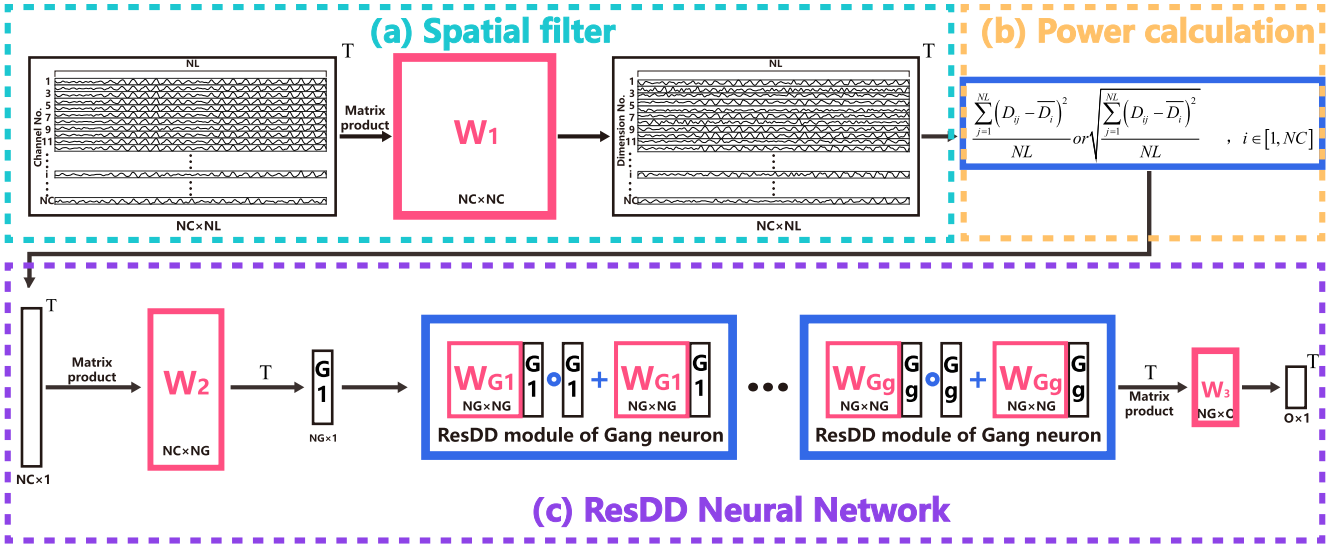

Fig. 2. EEGG model building for classification. (a) Spatial filter. (b) Power calculation. (c) ResDD Neural Network. EEGG Model is an end-to-end model, and the input of the EEGG model is the EEG data intercepted from a time window to be classified.The "Spatial filter" and "Power calculation" of EEGG refer to implementing the corresponding effects of previous single algorithms rather than using the corresponding single algorithms(e.g., CSP). *NC* : the number of channels. *NL* : the number of data points for each channel. *NG* : the dimensions of inputs of ResDD. *g* :the number of ResDD modules. *O* :the number of outputs. **Supplement: The DD neural network (Dendrite Net) is the basis for understanding EEGG(see [20] and [36]). It is the basic algorithm proposed by the author of this paper, and its properties have been proven through data sets in multiple fields.**

have been proved by experiments and theory (open source code) [20]. ResDD is an improved Dendrite Net using a residual strategy to prevent a vanishing gradient [36], [39]. ResDD inherits controllable nonlinear mapping and can be simplified after weight optimization because there is no nonlinear function in it. The work in this paper is the first application of the ResDD module of Gang neurons.

ResDD Neural Network in this paper contains a dimensionality reduction module, ResDD modules, and one linear module whose dimensions are determined by the number of categories. The role of the dimensionality reduction module is to project power $\boldsymbol{P}_i \in \mathbb{R}^{NC}$ onto NG dimensions to reduce computational complexity ($NG < NC$). The formula of the dimensionality reduction module is as follows.

$$\boldsymbol{P}^{G1} = (\boldsymbol{P}\boldsymbol{W}_2)^{\mathrm{T}} \tag{3}$$

where $\boldsymbol{P}^{G1} \in \mathbb{R}^{NG\times 1}$ expresses the outputs of the dimensionality reduction module. $\boldsymbol{W}_2 \in \mathbb{R}^{NC\times NG}$ is the weight matrix.

ResDD modules aim for nonlinear mapping. The degree of interaction terms is adjusted by the number of ResDD modules. The $i-$th ResDD module is expressed as follows.

$$\boldsymbol{P}^{Gi+1} = \boldsymbol{W}_{Gi}\boldsymbol{P}^{Gi} \circ \boldsymbol{P}^{Gi} + \boldsymbol{W}_{Gi}\boldsymbol{P}^{Gi}, \quad i \in [1, g],\ i \in \mathbb{N}^{+} \tag{4}$$

where $\boldsymbol{P}^{Gi} \in \mathbb{R}^{NG\times 1}$ and $\boldsymbol{P}^{Gi+1} \in \mathbb{R}^{NG\times 1}$ expresses the inputs and outputs of the $i-$ th ResDD module, respectively. $\boldsymbol{W}_{Gi} \in \mathbb{R}^{NG\times NG}$ is the weight matrix. $\circ$ expresses Hadamard product. It is noteworthy that ResDD modules do not contain nonlinear activation function, compared with the neuron in traditional artificial neural networks, which provides a prerequisite for simplifying the trained model.

The last linear module is used to achieve the mapping of category. The formula is as follows.

$$\boldsymbol{C}^{\mathrm{EEGGoutputs}} = \left(\boldsymbol{P}^{Gg+1}\right)^{T} \boldsymbol{W}_3 \tag{5}$$

where $\boldsymbol{P}^{Gg+1} \in \mathbb{R}^{NG\times 1}$ is the outputs of the last ResDD module. $\boldsymbol{P}^{\mathrm{EEGGoutputs}} \in \mathbb{R}^{1\times O}$ is the outputs of EEGG. The number of categories determines dimensions O. $\boldsymbol{W}_3 \in \mathbb{R}^{NG\times O}$ is the weight matrix.

B. Transformation of the Trained Model From the Classification Form to Relation Spectrum

This part aims to transform the trained EEGG model into simple components with physical meaning, which is similar to the purpose of Fourier transform (see Fig. 1 and Fig. 2). However, Fourier transform is used for signal decomposition, while EEGG is used to decompose the biological EEG-intention system. Since the DC component has been removed while building the EEGG model, the EEG variables of the EEGG model are regarded as the ideal state without the DC component. The power of EEG can be calculated by the magnitude squared instead of the variance or standard error. Therefore, neither Spatial filter, Power calculation, nor ResDD Neural Network contains a nonlinear function. Nevertheless, EEGG implements nonlinear operations by the Matrix product and Hadamard product. In order to "read" EEGG model that simulates the biological EEG-intention system, the input variables $\boldsymbol{E} = [E_1, E_2, \cdots, E_{NC}]$ and the output variable $C^{\mathrm{EEGGoutputs}}$ of system are set. Then, the trained EEGG model is represented by the formulae containing simple arithmetic operations according to the model building steps(see "*Model*

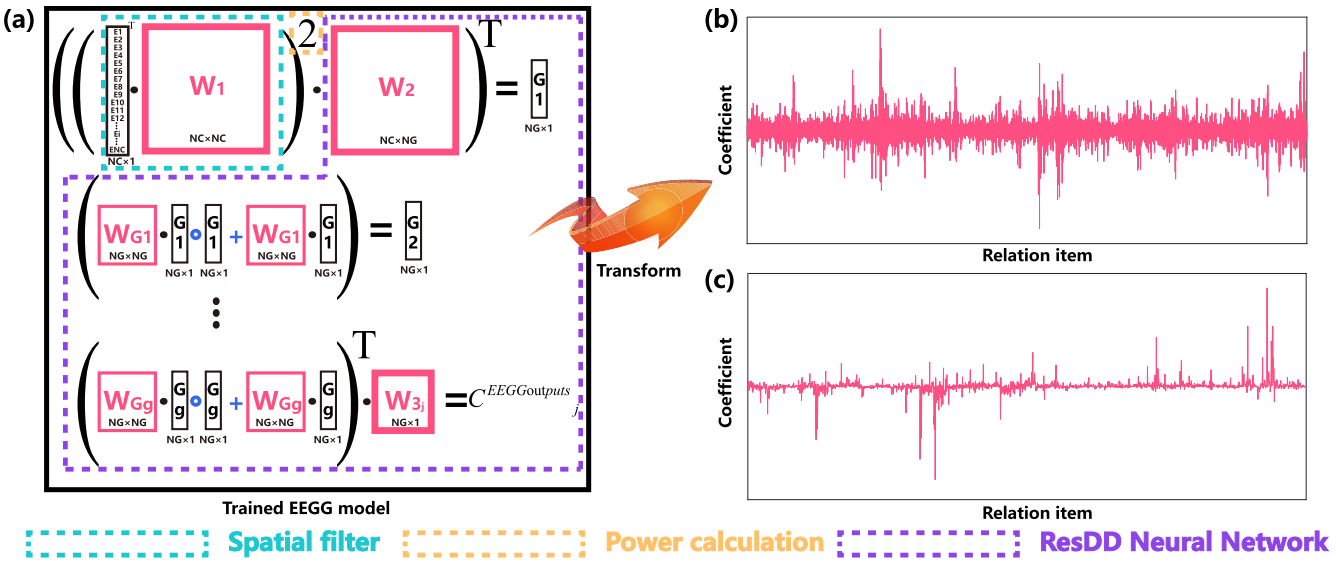

Fig. 3. Transformation of the trained model from the classification form to relation spectrum. (a) The transformation of the trained model. The step aims to transform the trained EEGG model into simple components with physical meaning. (b) The relation spectrum form of EEGG model. **By analogy to Fourier spectrum [abscissa: frequency *F* (i.e., complete form sin(2$\pi F t$) or cos(2$\pi F t$)).ordinate: amplitude (i.e., coefficient)], the abscissa of relation spectrum is items of independent components and interactive components [e.g., E_1 (first-order independent component), E_1^2 (second-order independent component), E_1E_2 (second-order interactive component), etc., where E_1 and E_2 are EEG signals.].** (c) The relation spectrum removing the odd items. Odd items: e.g.,E_1, $E_1^2E_2$, $E_1E_2^2$. Even items: e.g.,E_1^2, $E_1^2E_2^2$. C_i :the $i-$ th channel. *NC*: the number of channels. *NG* : the dimensions of inputs of ResDD. *g*:the number of ResDD modules. $C_j^{\text{EEGGoutpult}}$: the $j-$ th output.

building for classification" and Fig. 3).

$$\begin{cases} \boldsymbol{P}^{G1} = \left(\left(\boldsymbol{E}\boldsymbol{W}_1\right)^2 \boldsymbol{W}_2\right)^T \\ \boldsymbol{P}^{G2} = \boldsymbol{W}_{G1}\boldsymbol{P}^{G1} \circ \boldsymbol{P}^{G1} + \boldsymbol{W}_{G1}\boldsymbol{P}^{G1} \\ \quad\vdots \\ \boldsymbol{P}^{Gi+1} = \boldsymbol{W}_{Gi}\boldsymbol{P}^{Gi} \circ \boldsymbol{P}^{Gi} + \boldsymbol{W}_{Gi}\boldsymbol{P}^{Gi} \\ \quad\vdots \\ C^{EEGG\ \text{outputs}}{}_j = \left(\boldsymbol{W}_{Gg}\boldsymbol{P}^{Gg} \circ \boldsymbol{P}^{Gg} + \boldsymbol{W}_{Gg}\boldsymbol{P}^{Gg}\right)^T \boldsymbol{W}_{3_j} \end{cases} \tag{6}$$

where $\boldsymbol{W}_1 \in \mathbb{R}^{NC\times NC}$ is the weight matrix of the spatial filter. $\boldsymbol{W}_2 \in \mathbb{R}^{NC\times NG}$ is the weight matrix of the dimensionality reduction module. $\boldsymbol{W}_{G1} \in \mathbb{R}^{NG\times NG}, \ldots, \boldsymbol{W}_{Gi} \in \mathbb{R}^{NG\times NG}, \ldots, \boldsymbol{W}_{Gg} \in \mathbb{R}^{NG\times NG}$ are the weight matrixes of ResDD modules. $\left[\boldsymbol{W}_{3_1}\cdots\boldsymbol{W}_{3_j}\cdots\boldsymbol{W}_{3_O}\right] = \boldsymbol{W}_3 \in \mathbb{R}^{NG\times O}$ is the weight matrix of the last linear module for categories. $\boldsymbol{W}_{3_j} \in \mathbb{R}^{NG}$ denotes the weight vector of the $j-$ th output. $\boldsymbol{P}^{G1}, \ldots, \boldsymbol{P}^{Gi}, \ldots, \boldsymbol{P}^{Gg}$ are intermediate variables. g denotes the number of ResDD modules. $\circ$ expresses Hadamard product.

The weight matrixes in Eq.6 have been optimized by minimizing loss function using backpropagation during training the EEGG model. Therefore, the optimized weights are assigned to the corresponding matrixes or vectors in Eq.6. Then the relation spectrum was obtained by simplifying Eq.6 in software(e.g., Simplify Symbolic Expressions in MATLAB or Python).

Fig. 3b shows the relation spectrum form of the EEGG model. By analogy to Fourier spectrum, the abscissa of relation spectrum is items of independent components and interactive components. Because of the unsigned characteristic of EEG signals in the record, the effects of odd items are random. Thus, odd items are removed, and the new relation spectrum is shown in Fig.3c.

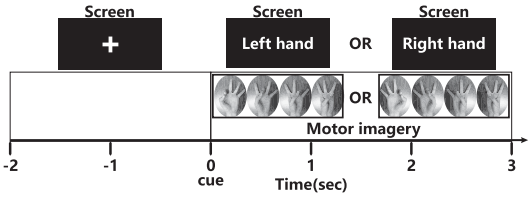

Fig. 4. Experimental paradigm [40], [41].

III. Experiments

A. Experimental Architecture

1) Q(1) EEGG's Advantages, Disadvantages, and Theoretical Reasons for the Performance: Firstly, this paper performed the statistical test on all subjects' classification results together (see Fig. 5). Secondly, in order to explore the advantages of EEGG deeper (to explore EEGG's advantages, disadvantages, and reasons), this paper divided the subjects into EEGG-advantaged and EEGG-disadvantaged groups (group (a) and group (b)). This paper explored the differences in algorithms within the group to determine whether the grouping is reasonable (see Fig. 6 and Fig. 7). Thirdly, this paper compared the differences between the EEGG-advantaged group(a) and EEGG-disadvantaged group(b) (see Fig. 8).

2) Q(2) Verification of ERD/ERS: Firstly, EEGG models were transformed into the new relation spectrum form. Then, this paper checked the number of relation items to verify whether the actual number matches the theoretical combination number. Secondly, in order to verify the universality

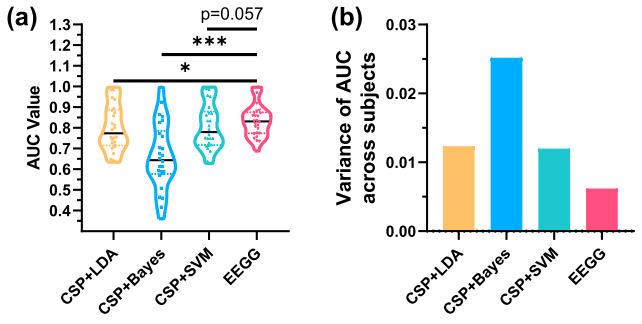

Fig. 5. Comparison between EEGG and other algorithms using all testing results. (a) Comparison in AUC. (b) Comparison in variance of the AUC. $^{*}p < 0.05.^{***}p < 0.001$.

and rationality of EEGG models, this paper computed the correlation matrix between the subjects' EEGG models (see Fig.9, Comparation of EEGG models). Last but not the least, in order to screen statistically significant items, one-sample t-tests under $p < 0.01$ and $p < 0.001$ were applied to compare each item's mean to zero (see Fig.10, statistical test of items across EEGG models, MATLAB code: *ttest*), because randomized effect approaches zero. Fig. 10 showed the items that differed significantly from zero. Further, this paper visualized the statistically significant items using the BrainNet Viewer ($p < 0.001$) (see Fig.11) [42].

The rationality of EEGG decomposition was verified by exploring whether the statistically significant items contained the known ERD/ERS phenomenon.

3) Q(3) Further Analysis Using EEGG: This paper analyzed the biological EEG-intention system based on the statistically significant items in the relation spectrum.

B. Experimental Details

1) Subjects: It is also well known that there is event-related desynchronization/synchronization (ERD/ERS) in the motor imagery paradigm [40], [43], [44]. Therefore, this paper used ERD/ERS in the MI paradigm to confirm EEGG's analysis capacity (The specific step is to verify whether the standard ERD and ERS phenomena can be found by "reading" the trained EEGG model instead of analyzing traditional EEG signals.). Additionally, there are many open MI datasets [40]. However, based on our knowledge of the MI paradigm, not all MI datasets notice essential details, such as BCI-inefficient subjects [24], inefficient MI [25], and mode of imagery [26]. Therefore, this paper selected the dataset [40] from GigaDB as we consider that this dataset took into account the above necessary details [40], [41]. This dataset contains EEG data of left- and right-hand motor imagery (MI) with 52 subjects. A 64-channel montage based on the international 10-10 system was used to record the EEG signals with 512 Hz sampling rate (see Fig. 11) [40]. Data with the noise electrodes and inefficient MI trials were marked. The most important detail was that subjects of this dataset were explicitly asked to imagine the kinesthetic experience rather than imagining the visual experience [26], [40]. Besides, an algorithm with high accuracy for a subject may perform terribly for other subjects, which is called a cross-subject problem [45]. Thus, this paper tested cross-subject accuracy. The following part of this paper will train a model for each subject to test the analytical performance of EEGG. Therefore, considering the number of models, we selected 1/2 of the dataset (26 subjects). Each subject was tested in turns. The testing subject's data were testing data, and other subjects' data were used to train models.

2) Data Preprocessing: Firstly, this paper removed the trial data with noise and intercepted the data from 0.5 s after the MI cue to 3 s(see Fig. 4). Secondly, the obtained data were filtered with a band-pass filter from 8 to 30 Hz. Finally, the obtained data were normalized between -1 and 1 in each trial. Besides, this problem was a two-class problem essentially, and thus this paper labeled the right-hand MI class as -1 and labeled the left-hand MI class as $+1$ [2]. The above procedure was repeated for data of all subjects. At this point, this paper obtained the data structure of every single trial of all subjects: EEG data $\boldsymbol{E} \in \mathbb{R}^{64\times1281}$, label $\boldsymbol{C} \in \mathbb{R}$.

3) EEGG Parameter and Contrast Models: According to the data structure of the single trial, the hyperparameters of EEGG were as follows: the number of channels NC was set as 64, the number of data points for each channel NL was set as 1281, the dimensions of inputs of ResDD NG was set as 2, the number of ResDD modules g was set as 1, the dimensions of outputs O was set as 1.

This paper did not emphasize that the classification accuracy of EEGG was better than the state of the art (SOTA) and mainly emphasized EEGG's decomposition capability. Therefore, this paper selected three typical "CSP+" BCI algorithms as contrast models: CSP and LDA (CSP+LDA), CSP and Naive Bayes classifier (CSP+Bayes), and CSP and SVM (CSP+SVM). Contrast models was actualized via CSP Toolbox and Statistics and Machine Learning Toolbox in MATLAB R2019a (CSP code: *csp*, LDA code: *fitcdiscr*, Bayes code: *fitcnb*, SVM code: *fitcsvm*). Among them, the SVM used a radial basis function Kernel (RBF).

4) Classification Performance: The receiver operating characteristic (ROC) curve and the area under the curve (AUC) were used for performance measures [2]. Besides, because this study aims to compare the differences between EEGG and other algorithms, and the data for comparing EEGG with other algorithms were paired, this paper used a paired-sample t-test. Of note, this paper did not care about the differences between other algorithms. Thus, it was essentially a pairwise comparison between both groups (EEGG vs. CSP+LDA, EEGG vs. CSP+Bayes, EEGG vs. CSP+SVM).

This paper performed three statistical analyses. Firstly, this paper compared the AUC and variance of the AUC of EEGG with other algorithms using all subjects' testing results (see Fig.5). Secondly, the subjects were partitioned into group (a) and group (b) based on whether EEGG outperformed others (see Fig.6). This paper compared the AUC of EEGG with other algorithms within group (a) and group (b) (see Fig.7). Thirdly, this paper compared the AUC between both groups (see Fig.8).

IV. Results

These results were annotated according to the experimental architecture.

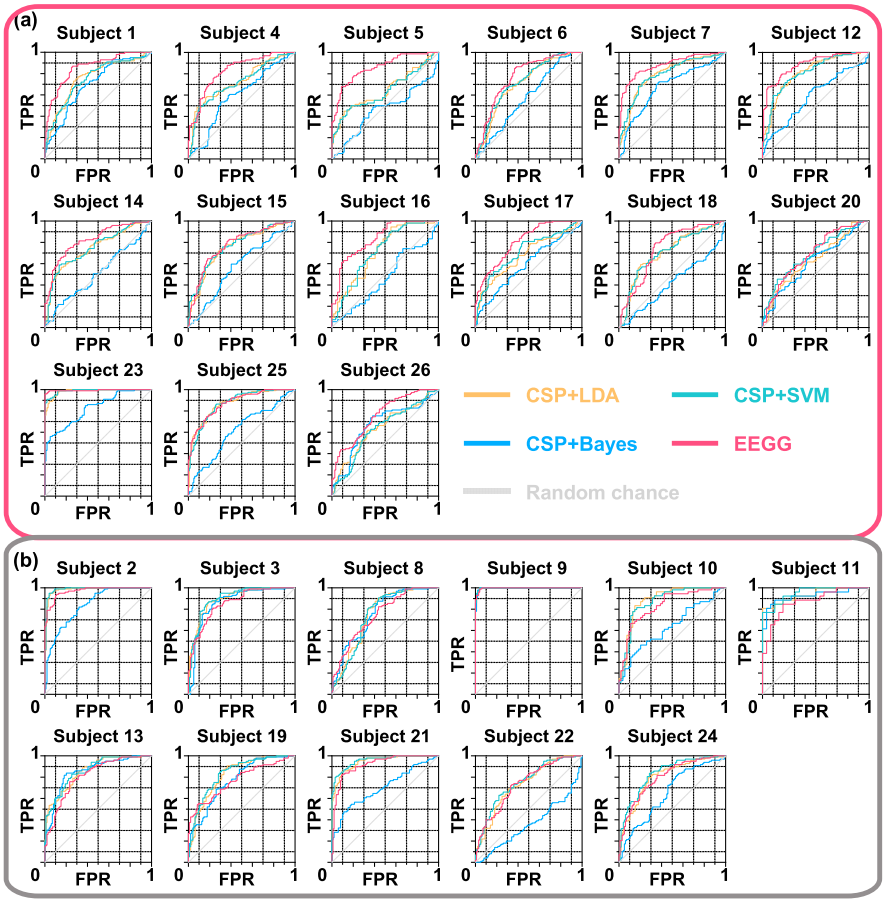

Fig. 6. Partition based on whether EEGG outperformed others. (a) EEGG-advantaged group. (b) EEGG-disadvantaged group. These above figures were ROC curves. TRP: True Positive Rate. FRP: False Positive Rate.

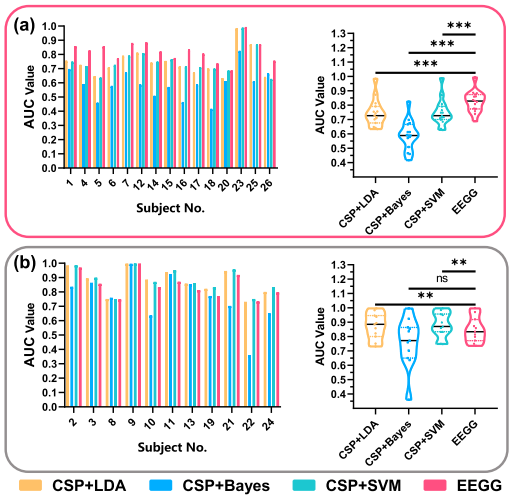

Fig. 7. Comparison between EEGG and other algorithms within groups. (a) Comparison within group (a). (b) Comparison within group (b). Note that the group is a control variable. $^{**}p < 0.01.^{***}p < 0.001.ns > 0.05$.

A. Classification Performance

1) Results of Q(1)-EEGG's Advantages, Disadvantages, and Theoretical Reasons for the Performance: The purpose of this experiment was to explore classification performance. Fig. 5a showed that EEGG significantly outperformed CSP+LDA and CSP+Bayes and might outperform CSP+SVM. [AUC, Paired-samples t-test: $0.834 \pm 0.079(EEGG) > 0.800 \pm 0.111(CSP + LDA)$, $p < 0.05$; $0.834 \pm 0.079(EEGG) > 0.662 \pm 0.159(CSP + Bayes)$, $p < 0.001$; $0.834 \pm 0.079(EEGG) > 0.806 \pm 0.109(CSP + SVM)$, $p = 0.057$] What stands out in Fig. 5a was that EEGG's AUC appeared to be more concentrated. Therefore, this paper compared the variance of AUC among algorithms. Interestingly, the variance of AUC of EEGG is smaller than others, which means that EEGG maybe has better robustness (see Fig.5b, Smaller variance means that the number of testing results deviating from the mean is relatively lower.).

Further analysis was necessary for EEGG's advantages and disadvantages. This paper divided the testing results of the subjects into both groups based on whether EEGG outperformed others (see Fig.6). To determine whether the grouping is reasonable, further analysis of the data within the group revealed that EEGG significantly outperformed others in the EEGG-advantaged group (a), "CSP+" significantly outperformed EEGG in the EEGG-disadvantaged group (b) except for CSP+Bayes. [see Fig. 7. Group (a), AUC, Paired-samples t-test: $0.825 \pm 0.074 > 0.745 \pm 0.094$, $p < 0.001$; $0.825 \pm 0.074 > 0.591 \pm 0.104, p < 0.001$; $0.825 \pm 0.074 > 0.750 \pm 0.091$, $p < 0.001$. Group (b), AUC, Paired-samples t-test: $0.847 \pm 0.087 < 0.873 \pm 0.090, p < 0.01$; $0.847 \pm 0.087 > 0.760 \pm 0.173$, $p = 0.061$; $0.847 \pm 0.087 < 0.881 \pm 0.087$, $p < 0.01$.].

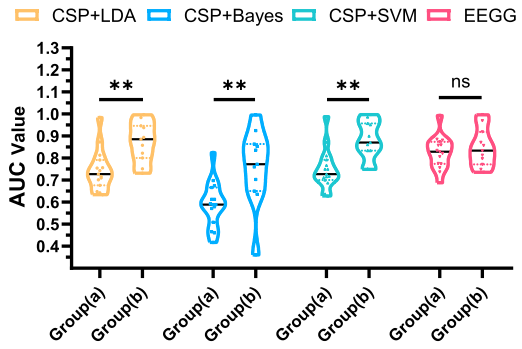

Fig. 8. Comparison between groups. Note that the algorithm is a control variable. $^{**}p < 0.01.ns > 0.05$.

If we now turn to Fig. 8, the subjects' data in group (b) were easier to classify correctly (see Fig. 8). There were only two reasons determining classification performance: algorithm and data itself. Therefore, we regarded an algorithm as a control variable. The AUC value of group (b) is higher than that of group (a) under the same algorithm (e.g., CSP+LDA), which implies that this means group (b) data has more effective information for classification, and group (a) data contains more noise (see Fig. 8). Further, there were significant differences in "CSP+" between group (a) and group (b) (see Fig. 8). However, EEGG results showed no significant differences between groups (see Fig. 8). This implies that "CSP+" algorithms in this paper were more sensitive to the quality of EEG data. They exhibited better classifier performance than EEGG for good-quality data, and they performed poorly than EEGG for low-quality data. In other words, EEGG was not sensitive to the quality of EEG data than "CSP+" algorithms. Although EEGG did not exhibit the highest classification accuracy, it performed better than others for low-quality data (see Fig. 8). [AUC, Paired-samples t-test: CSP+LDA:$0.745 \pm 0.094 < 0.873 \pm 0.090$, $p < 0.01$; CSP+Bayes:$0.591 \pm 0.104 < 0.760 \pm 0.173$, $p < 0.01$; CSP+SVM: $0.750 \pm 0.091 < 0.881 \pm 0.087$, $p < 0.01$;EEGG: $0.825 \pm 0.074 < 0.847 \pm 0.087$, $p = 0.499$.]

Taken together, these above statistical analyses provided important insights that EEGG has better robustness for low-quality EEG data (see Fig.6, Fig.7, and Fig.8).

In addition, we extended EEGG to all data in the GigaDB dataset to explore the classification accuracy. TABLE II shows the comparison of classification accuracy between EEGG and recent algorithms. EEGG exhibits moderate improvement for low-quality EEG signals relative to some algorithms (e.g., comparison between EEGG and "CSP+" algorithms). Using eleven real-world datasets obtained from different fields, we have demonstrated that DD's generalization capability is better than some basic machine learning algorithms, such as Multilayer Perceptron(MLP) and SVM, in the literature [20]. The core module of EEGG is the DD module. The result in TABLE II is consistent with DD in the literature [20]. Nevertheless, we acknowledge that the classification accuracy of EEGG is lower than some deep learning algorithms. It is difficult for us to create an algorithm with the best excellent performance in all aspects. The learned EEGG model or simulated brain system can be analyzed like a transfer function

TABLE II
CLASSIFICATION ACCURACY COMPARISON BETWEEN EEGG AND RECENT ALGORITHMS

Algorithm	Accuracy for all data	Accuracy for good-quality EEG signals	Accuracy for low-quality EEG signals
DeepConvNet+VMD+STFT [48]	$88.51 \pm 10.64\%$	$89.67 \pm 8.34\%$	$87.36 \pm 12.55\%$
EEGNet+VMD+STFT [48]	$85.66 \pm 7.49\%$	$85.18 \pm 7.06\%$	$86.16 \pm 8.02\%$
EEGNet+STFT [48]	$72.63 \pm 10.27\%$	$74.67 \pm 10.49\%$	$70.60 \pm 9.86\%$
AlexNet+VMD+STFT [48]	$71.82 \pm 13.55\%$	$79.42 \pm 12.27\%$	$64.23 \pm 10.20\%$
LeNet+VMD+STFT [48]	$70.72 \pm 7.88\%$	$76.98 \pm 4.7\%$	$64.47 \pm 4.82\%$
CSP+LDA	$76.30 \pm 9.99\%$	$82.89 \pm 9.27\%$	$71.46 \pm 7.58\%$
CSP+Bayes	$66.25 \pm 11.77\%$	$73.90 \pm 13.20\%$	$60.64 \pm 6.58\%$
CSP+SVM	$76.59 \pm 9.80\%$	$83.15 \pm 8.75\%$	$71.77 \pm 7.62\%$
EEGG(Our)	$78.09 \pm 8.20\%$	$79.61 \pm 9.11\%$	$76.97 \pm 7.60\%$

The EEG data whose classification accuracy of LeNet+VMD+STFT are ranked on top 50 % are regarded as good-quality EEG signals, and the other half are regarded as low-quality EEG signals. Dataset: GigaDB dataset. Data:$mean \pm std$.

in cybernetics [46], [47], which is the unique feature of EEGG and the main contribution of this paper to the BCI algorithm field.

B. Transformation of EEGG Model and Analysis of Relation Spectrum

This section is divided into three parts: (1) Transformation of EEGG models and correctness validation, (2) statistical analysis of relation items in relation Spectrum and correctness validation using the known ERD/ERS phenomenon, and (3) the further BCI-based analysis of brain using relation spectrum.

Fig. 9 showed the EEGG models that were transformed into the relation spectrum without odd items. The abscissa (P) of Fig. 9a is E^2, where E was EEG signal. In order to verify the correctness of items, this paper first calculated the total number of pairwise interaction items, independent powers items, and the squared of independent powers items by combination in mathematics$\left(C_{64}^2 + 64 + 64 = 2144\right)$. Then this paper calculated the correlation matrix between subjects' EEGG models (see Fig. 9b). The theoretical combination number was equal to the number of items in the relation spectrum (see Fig. 9a). The relation spectrums were similar across EEGG models (see Fig. 9).

1) Results of Q(2)-Verification of ERD/ERS: Turning now to the statistical analysis of relation spectrums, we found some significant regularities, such as the symmetry of relation items (see Fig. 10). In order to make the regularities more intuitional, this paper visualized the relation spectrum (i.e., EEGG model) using the BrainNet Viewer (see Fig. 11). **"Ball" expresses the independent components of brain regions, and "rod" expresses the interactive components of brain regions.** The effects of "red ball," "blue ball," "blue rod," and "red rod" in Fig. 11a can be expressed as follows, respectively.

$$\begin{cases} y^{\text{redball-effect}} = k_{\text{redball}}\, P_{\text{redball}} \quad \text{(see Fig.11b)} \\ y^{\text{blueball-effect}} = -k_{\text{blueball}}\, P_{\text{blueball}} \quad \text{(see Fig.11c)} \\ y^{\text{bluerod-effect}} = -k_{\text{bluerod}} P_{\text{bluerod-ball1}}\, P_{\text{bluerod-ball2}} \quad \text{(see Fig.11d)} \\ y^{\text{redrod-effect}} = k_{\text{redrod}}\, P_{\text{redrod-ball1}} P_{\text{redrod-ball2}} \quad \text{(see Fig.11e)} \end{cases} \tag{7}$$

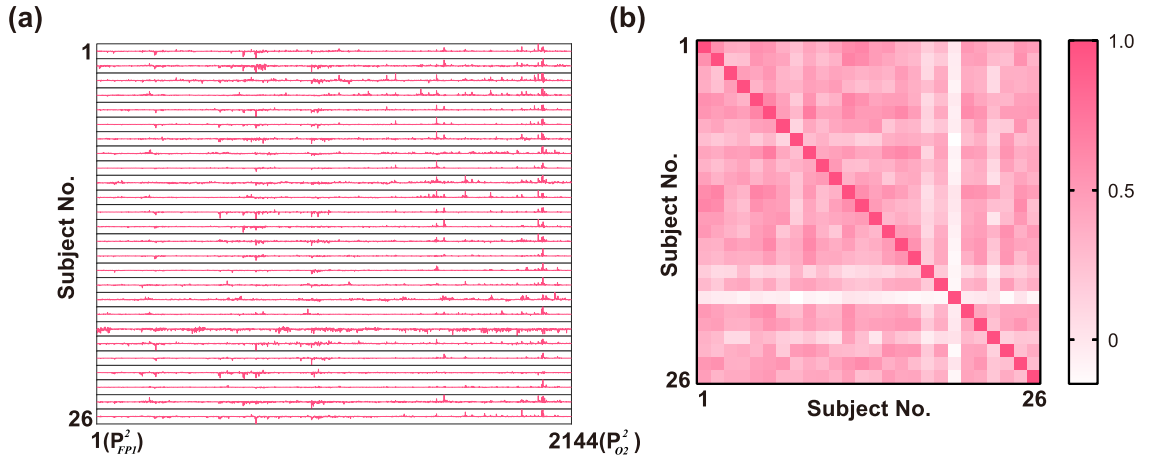

Fig. 9. Transformed EEGG models. (a) The relation spectrum without odd items. (b) Correlation matrix between subjects' EEGG models. $P = E^2$, where E is EEG signal.

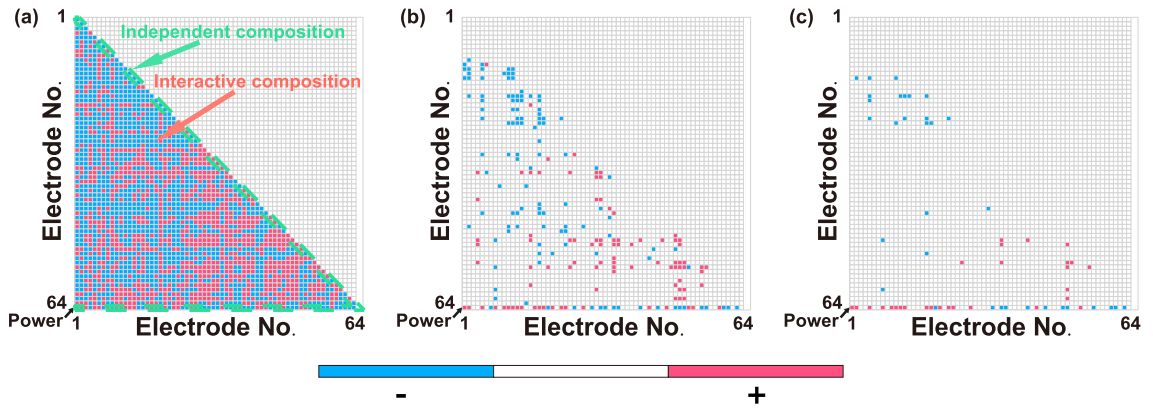

Fig. 10. Results of statistical analysis of relation items in EEGG models. (a) Mean of relation items in EEGG models. (b) Results of statistical analysis under $p < 0.01$. (c) Results of statistical analysis under $p < 0.001$. "+": Positive effect. "−": Negative effect. Note that the electrode number in the above figures corresponds to the label in Fig. 11, and the upper triangular matrixes were not used.

where $y^{\text{redball-effect}}$, $y^{\text{blueball-effect}}$, $y^{\text{bluerod-effect}}$, and $y^{\text{redrod-effect}}$ expresses the effects of "red ball," "blue ball," "blue rod," "red rod," respectively. $k_{\text{redball}} \in \mathbb{R}^+$, $k_{\text{blueball}} \in \mathbb{R}^+$, $k_{\text{bluerod}} \in \mathbb{R}^+$, and $k_{\text{redrod}} \in \mathbb{R}^+$ are proportional coefficients. $P_{\text{redball}} \in [0, 1]$, $P_{\text{blueball}} \in [0, 1]$, $P_{\text{bluerod-ball1}} \in [0, 1]$, $P_{\text{bluerod-ball2}} \in [0, 1]$, $P_{\text{redrod-ball1}} \in [0, 1]$, and $P_{\text{redrod-ball2}} \in [0, 1]$ represents powers. P_{redball} and P_{blueball} express the independent components. $P_{\text{bluerod-ball1}}$ $P_{\text{bluerod-ball2}}$ and $P_{\text{redrod-ball1}}$ $P_{\text{redrod-ball2}}$ express the interactive components. In order to show the change of the above effects, this paper plotted the graphs when proportional coefficients were 1(see Fig. 11b, Fig. 11c, Fig. 11d, and Fig. 11e).

Next, this paper verified the known ERD/ERS phenomenon and showed a new phenomenon [44]. In the subsequent analysis, we assume that the subject performs left-hand MI and takes the real left-hand MI situation as an example to verify the relation spectrum and analyze the human brain. When the subject performs left-hand MI, the power of the right hemisphere will decrease (ERD), and the power of the left hemisphere will increase (ERS) according to the known ERD/ERS phenomenon [44].The left-hand MI represents positive in the EEGG model. If the relation spectrum was reasonable, the EEGG model's output would tend to be positive when the ERD/ERS phenomenon of left-hand MI occurs (That is, this brain state tends to be classified as left-hand MI by the EEGG model or relation spectrum.).

It happened that most "blue balls" distribute on the right hemisphere, and most "red balls" distribute on the left hemisphere (see Fig. 11a). The EEGG model's output increases with decreasing power of "blue ball" (see yellow arrow in Fig. 11c), in which decreasing power of "blue ball" is the ERD. Likewise, the EEGG model's output increases with increasing power of "red ball" (see yellow arrow in Fig. 11b), in which increasing power of "red ball" is the ERS.

2) Results of Q(3)-Further Analysis Using EEGG: Additionally, it happened that most "red rods" distribute on the right hemisphere, and most "blue rods" distribute on the left hemisphere (see Fig. 11a). The effects of "rods" put a brake on the effects of "balls." In Fig. 11e, we found the EEGG model's output decreases with decreasing power in both ends of "red rod" (see yellow arrow in Fig. 11e). In Fig. 11d, we found the EEGG model's output decreases with increasing power in both ends of "blue rod" (see yellow arrow in Fig. 11d). In order to slow the rate of decline, the power of both connected "balls" should not change at the same time as

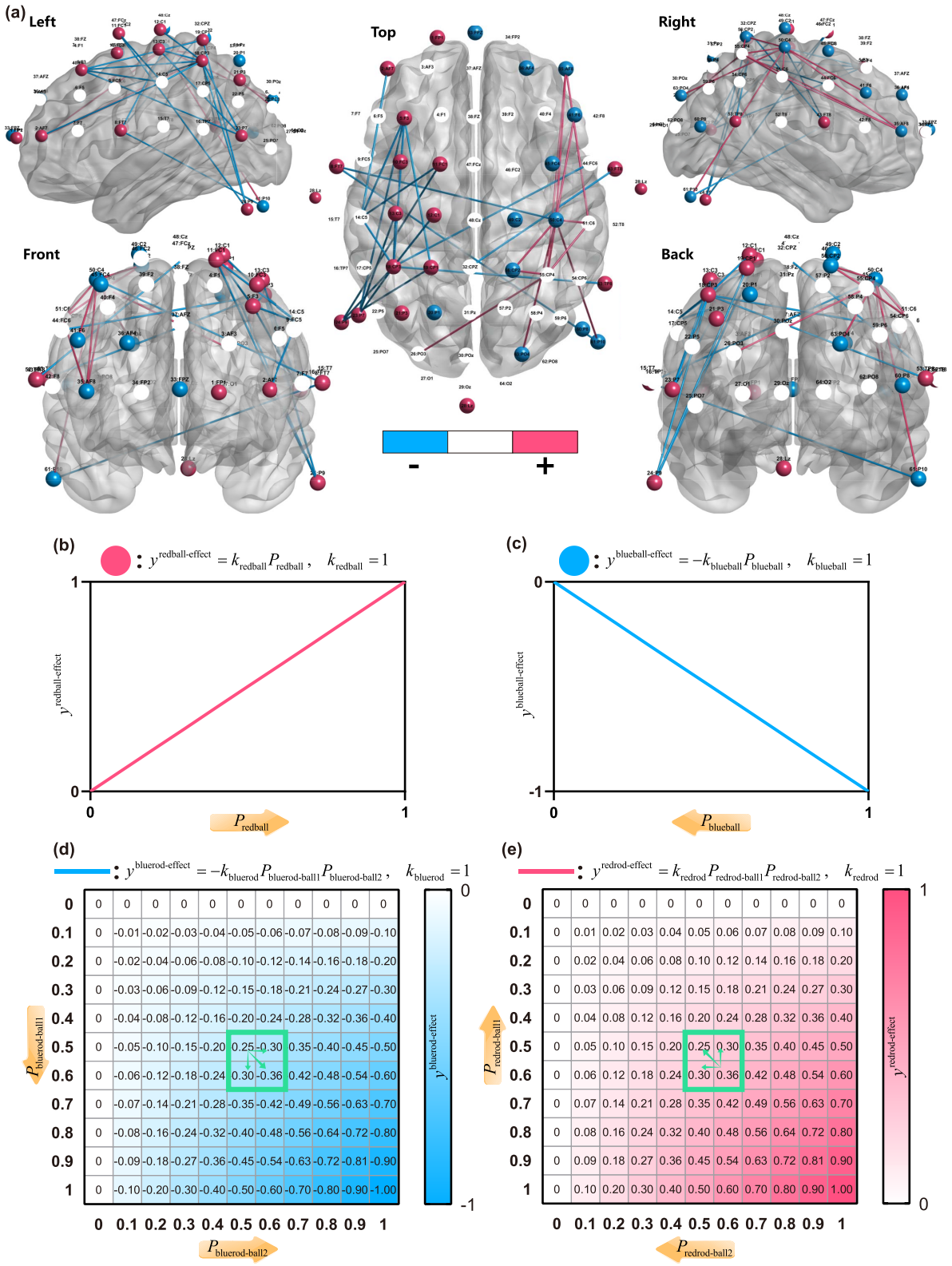

Fig. 11. Visualization of the EEGG model under $p < 0.001$. (a) The EEGG model. "Ball" expresses the independent components of brain regions, and "rod" expresses the interactive components of brain regions. (b) Graph of the effects of "red ball" in (a). (c) Graph of the effects of "blue ball" in (a). (d) Graph of the effects of "blue rod" in (a). (e) Graph of the effects of "red rod" in (a). Fig. 11b, c, d, e were the graph of Eq.7 for describing the effects of relation items.

possible because the most gradient was on the diagonal line (see Fig. 11d and Fig. 11e). In other words, the power in large areas should not change simultaneously so that the brain status can be identified as left-hand MI. This implies that the activation in the brain should be more centralized for fine intentions.

Supplement for understanding the "rod" in Fig. 11 : The "rod" represents the effect of the simultaneous change of the "balls" at both ends of the "rod" on the category(see Fig.11d and Fig. 11e). The "ball" represents the power of the corresponding brain regions. Thus, the "rod" represents the effect of the simultaneous power change of both brain regions on the category.

V. Discussion

The human brain is a complex interconnected dynamical system [49]. Since the first BCI has been proposed, efforts were then paid to decipher the human brain. This paper presents the analytic "white box" Brain-computer interface algorithm named EEGG that decomposed the biological EEG-intention system into relation spectrum (Taylor-like series) for the first time, which offers a novel frame for analyzing the brain. Through the experiments, this paper explored the classification performance of EEGG, verified the rationality of the relation spectrum, and then tried to analyze further the brain based on the relation spectrum.

The following theoretical analysis explained the results.

A. The Controllable Logical Expression Capacity of EEGG Makes It Better Robust for Low-Quality EEG Data

EEG is the most common brain signal that has been utilized in BCI applications because of its non-invasive nature and low cost [50], [51]. However, EEG has a low signal-to-noise ratio [32], [50], [51]. Most ML algorithms aim to get more excellent expression ability [52]. Nevertheless, the EEG-BCI model using ML algorithms with too excellent expression ability is easy to be over-fitting for the low-quality EEG data. EEG-ML algorithms should just enough express a small amount of classified information and do not have the ability to express a large amount of other information(e.g., noise). That is, the ML algorithm with outstanding approximation or expression ability may not be suitable for the low-quality EEG data (see TABLE II).

The expressive ability of the EEG-BCI model should be artificially set for better robustness. Dendrite Net presented by Gang Liu *et al.* in 2020 has controllable logical expression capacity, which happens to meet the needs of EEG [20]. Dendrite Net aims to design the logical extractor with controllable logical expression capacity. And its logical expression capacity can be adjusted by the number of dendrite modules.

In this paper, we used the enhanced DD, ResDD of Gang neurons [36]. ResDD is an improved Dendrite Net using a residual strategy to prevent a vanishing gradient. The logical expression capacity of ResDD modules is the same as the DD module. After the logical expression capacity of EEGG model is set, it remains constant. The constant logical expression capacity made the EEGG model avoid the overfitting and improved the robustness for low-quality EEG data (see Fig. 8 and TABLE II, a schematic visualization is shown in Fig. 12.). Meanwhile, the corresponding disadvantage is that the constant logical expression capacity cannot express some details and made EEGG not exhibit the highest classification accuracy for good-quality EEG data (see Fig. 8). Fortunately, the logical expression capacity of EEGG is controllable. Thus, researchers can adjust it based on the actual conditions.

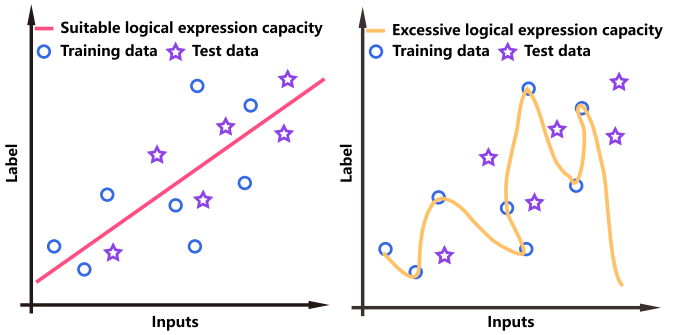

Fig. 12. Schematic visualization of logical expression capability. The logical expression capacity is set as a constant, which may be the reason for the moderate improvement in classification from EEGG for low-quality EEG signals.

B. The Biological EEG-Intention System was Decomposed Into Taylor-Like Series

EEGG model consists of Spatial filter, Power calculation, and ResDD Neural Network. In the transformation of EEGG model, the power of EEG was calculated by the magnitude squared instead of the variance or standard error(nonlinear function). Besides, Neither Spatial filter nor ResDD Neural Network contains a nonlinear function [16], [36]. EEGG only contains Matrix product and Hadamard product, although it implemented nonlinear operations. Therefore, the relation spectrum can be obtained by simplifying Eq.6 in software(e.g., Simplify Symbolic Expressions in MATLAB or Python). Besides, we recommend choosing as few ResDD modules as possible to generate a small number of components in order to analyze the physical meaning easier, such as the fourth-order of EEG(the second-order of EEG is the EEG power).

This paper found the known ERD/ERS phenomenon in the relation spectrum and verified the correctness of the EEGG analysis. Further, based on the relation spectrum, it was concluded that generating fine hand intention needs more centralized activation in the brain (see Fig. 11). In other words, fine motion corresponded to a centralized region. This finding was similar to the anatomy study [53].

C. Decomposition of the Biological EEG-Intention System

"Decomposition" refers to decomposing an unknown complex composition into some simple components with physical meaning (e.g., Fourier transform and Fourier spectrum for decomposing signals) and read parameters of the white-box model(i.e., simple components) [19].

This paper emphasized the decomposition of the biological EEG-intention system. A functional relation can be expressed by the sum of trigonometric or power polynomial. For the expression of a trigonometric polynomial, the typical example is Fourier frequency spectrum. Here, the relation spectrum is the spectrum of the power series. For the analysis, EEGG can be understood by analogy to Fourier transform. However, Fourier Transform was used for signal decomposition, while

TABLE III
EEGG'S ADVANTAGES AND DISADVANTAGES FOR DIFFERENT REQUIREMENTS

Requirement	EEGG	Other complex algorithms
Analyzing the trained model/brain	Yes	No
Lower computational complexity	Yes	No
Poor data quality and needing moderate generalization	Yes	-
Good data quality and needing the highest classification accuracy	No	Yes

EEGG was used to decompose the biological EEG-intention system. From the perspectives of cybernetics, a transfer function of a system, sub-system, or component is a mathematical function that theoretically models the system's output for each possible input and is used to analyze and identify the real system [46], [47]. The trained EEGG model can be regarded as a transfer function of the biological EEG-intention system.

In addition, here we add some discussion about the characteristics of EEG signals. EEG signals often contain lots of unknown components. These unknown components are also independent or interactive compositions for the biological EEG-intention system. During the training stage of the EEGG model, the weight of the interference or uncorrelated compositions for the category will be optimized to a small value to higher classification accuracy. Therefore, in the relation spectrum, the uncorrelated compositions for the category are a small value close to 0. Besides, PCA and ICA are common methods for getting independent components or filtering uncorrelated components in EEG signals themselves. However, it is worth noting that the concept of the independent components of ICA is different from the independent components in EEGG. PCA and ICA aim to separate EEG data by unsupervised strategy, and the independent components in ICA are unrelated to the category of classification. EEGG aims to separate the biological EEG-intention system by supervised strategy, and the independent components in EEGG are based on the category of classification and are the independent components of the EEG-intention system.

D. Some Additional Discussion

Algorithms in online applications, especially in engineering, will consider computational complexity and running speed, and low time complexity means less delay. Compared with traditional neural networks, ResDD Neural Network in EEGG uses Hadamard product instead of a non-linear function, which is similar to DD(see Fig. 2) [20]. Hadamard product has lesser computational complexity than a non-linear function. Thus, EEGG often has lesser computational complexity than other neural networks. Furthermore, TABLE III shows EEGG's advantages and disadvantages for different requirements.

There are also limitations in this paper. This paper did not emphasize that the classification accuracy was better than SOTA for some datasets, it paid more attention to the specific characters in theoretical proof (the controllable logical expression capacity for classification) and mainly emphasized EEGG's analysis capacity. This paper is the first decomposition with Taylor-like series on the biological EEG-intention system. EEGG can decompose the brain intentions (system), just like the Fourier transform decomposes signal. Additionally, in order to verify the correctness of the EEGG analysis, this paper selected the MI paradigm with the known ERD/ERS phenomenon. Additionally, multiclass classification using EEGG will be explored in future research. Because the correctness of the transformed EEGG model(relation spectrum) has been verified and the transformation was the same for both and multiclass classification, the multiclass EEGG models can be analyzed in future research. In addition, this paper is the initial verification of the algorithm in the basic principle, and we only verified the algorithm's performance from the Left- and right-hand MI paradigm. EEGG will be used in different experimental paradigms and different fields, such as emotion classification and depression identification, in the future.

VI. CONCLUSION

A "white box" brain-computer interface algorithm named EEGG that decomposed the biological EEG-intention system into relation spectrum (Taylor-like series) was proposed in the paper, which offers a novel frame for analysis of the brain. EEGG can be used for intention recognition and analyzing the biological EEG-intention system. The conclusions of major questions of the algorithm/frame proposed in the Introduction section are as follows.

(1) Experiments and theoretical analysis showed EEGG had better robustness for low-quality EEG data.
(2) Experiments proved the known ERD/ERS existed in the relation spectrum, and the relation spectrum was reasonable.
(3) Based on the relation spectrum, this paper found that generating fine hand intention needs more centralized activation in the brain.

Before closing, it is worth mentioning that decomposing biological EEG-intention systems into Taylor-like series via EEGG may find some important findings of the brain in the future, and this paper is the foundation.

ACKNOWLEDGMENT

The authors would like to thank the researchers who contacted them, discussed with them, and offered suggestions for their preprint; the editor; and the anonymous reviewers for their valuable comments on improving the paper. These suggestions improved previous manuscript. Code could be found at *GitHub: Gang neuron:* https://github.com/liugang1234567/Gang-neuron.

REFERENCES

[1] M. A. L. Nicolelis, "Actions from thoughts," *Nature*, vol. 409, pp. 403–407, Jan. 2001.
[2] F. Lotte *et al.*, "A review of classification algorithms for EEG-based brain–computer interfaces: A 10 year update," *J. Neural Eng.*, vol. 15, no. 3, Jun. 2018, Art. no. 031005.
[3] Y. Jiao, Y. Zhang, X. Chen, E. Yin, J. Jin, X. Wang, and A. Cichocki, "Sparse group representation model for motor imagery EEG classification," *IEEE J. Biomed. Health Inform.*, vol. 23, no. 2, pp. 631–641, Mar. 2018.
[4] S. Kumar, R. Sharma, and A. Sharma, "OPTICAL+: A frequency-based deep learning scheme for recognizing brain wave signals," *PeerJ Comput. Sci.*, vol. 7, p. e375, Feb. 2021.

[5] O. Lo-Thong *et al.*, "Identification of flux checkpoints in a metabolic pathway through white-box, grey-box and black-box modeling approaches," *Sci. Rep.*, vol. 10, no. 1, pp. 1–19, Dec. 2020.

[6] X. Li and J. Wen, "Review of building energy modeling for control and operation," *Renew. Sustain. Energy Rev.*, vol. 37, pp. 517–537, Sep. 2014.

[7] X. Wang and O. Gotoh, "Accurate molecular classification of cancer using simple rules," *BMC Med. Genomics*, vol. 2, no. 1, pp. 1–23, Dec. 2009.

[8] Y. Jiao, T. Zhou, L. Yao, G. Zhou, X. Wang, and Y. Zhang, "Multi-view multi-scale optimization of feature representation for EEG classification improvement," *IEEE Trans. Neural Syst. Rehabil. Eng.*, vol. 28, no. 12, pp. 2589–2597, Dec. 2020.

[9] Q. Wang, G. M. Garrity, J. M. Tiedje, and J. R. Cole, "Naive Bayesian classifier for rapid assignment of rRNA sequences into the new bacterial taxonomy," *Appl. Environ. Microbiol.*, vol. 73, no. 16, pp. 5261–5267, Aug. 2007.

[10] C. Zhang and A. Eskandarian, "A computationally efficient multi-class time-frequency common spatial pattern analysis on EEG motor imagery," in *Proc. 42nd Annu. Int. Conf. IEEE Eng. Med. Biol. Soc. (EMBC)*, Jul. 2020, pp. 514–518.

[11] D. Erhan, Y. Bengio, A. Courville, and P. Vincent, "Visualizing higher-layer features of a deep network," *Univ. Montreal*, vol. 1341, no. 3, p. 1, 2009.

[12] M. D. Zeiler and R. Fergus, "Visualizing and understanding convolutional networks," in *Computer Vision—ECCV 2014*, D. Fleet, T. Pajdla, B. Schiele, and T. Tuytelaars, Eds. Cham, Switzerland: Springer, 2014, pp. 818–833.

[13] L. Van der Maaten and G. Hinton, "Visualizing data using t-SNE," *J. Mach. Learn. Res.*, vol. 9, no. 11, pp. 1–27, 2008.

[14] I. Sturm, S. Lapuschkin, W. Samek, and K.-R. Müller, "Interpretable deep neural networks for single-trial EEG classification," *J. Neurosci. Methods*, vol. 274, pp. 141–145, Dec. 2016.

[15] M. R. Joglekar, L. Chariker, R. Shapley, and L.-S. Young, "A case study in the functional consequences of scaling the sizes of realistic cortical models," *PLOS Comput. Biol.*, vol. 15, no. 7, Jul. 2019, Art. no. e1007198.

[16] G. Liu and J. Wang, "A relation spectrum inheriting Taylor series: Muscle synergy and coupling for hand," *Frontiers Inf. Technol. Electron. Eng.*, vol. 23, no. 1, pp. 145–157, Jan. 2022, doi: 10.1631/FITEE.2000578.

[17] G. P. Tolstov, *Fourier Series*. New York, NY, USA: Dover, 1962.

[18] R. N. Bracewell and R. N. Bracewell, *The Fourier Transform and its Applications*, vol. 31999. New York, NY, USA: McGraw-Hill, 1986.

[19] P. D. Welch, "The use of fast Fourier transform for the estimation of power spectra: A method based on time averaging over short, modified periodograms," *IEEE Trans. Audio Electroacoust.*, vol. AE-15, no. 2, pp. 70–73, Jun. 1967.

[20] G. Liu and J. Wang, "Dendrite net: A white-box module for classification, regression, and system identification," *IEEE Trans. Cybern.*, early access, Nov. 18, 2021, doi: 10.1109/TCYB.2021.3124328.

[21] A. Backlund, "The definition of system," *Kybernetes*, vol. 29, no. 4, pp. 444–451, 2000.

[22] S. E. Petersen and M. I. Posner, "The attention system of the human brain: 20 years after," *Annu. Rev. Neurosci.*, vol. 35, pp. 73–89, Jan. 2012, doi: 10.1146/annurev-neuro-062111-150525.

[23] S. Liu *et al.*, "What makes a good movie trailer? Interpretation from simultaneous eeg and eyetracker recording," in *Proc. 24th ACM Int. Conf. Multimedia*, 2016, pp. 82–86.

[24] X. Shu *et al.*, "Fast recognition of BCI-inefficient users using physiological features from EEG signals: A screening study of stroke patients," *Frontiers Neurosci.*, vol. 12, p. 93, Feb. 2018.

[25] R. Zhang *et al.*, "Efficient resting-state EEG network facilitates motor imagery performance," *J. Neural Eng.*, vol. 12, no. 6, Dec. 2015, Art. no. 066024.

[26] C. Neuper, R. Scherer, M. Reiner, and G. Pfurtscheller, "Imagery of motor actions: Differential effects of kinesthetic and visual–motor mode of imagery in single-trial EEG," *Cognit. Brain Res.*, vol. 25, no. 3, pp. 668–677, 2005.

[27] F. Lotte, M. Congedo, A. Lécuyer, F. Lamarche, and B. Arnaldi, "A review of classification algorithms for EEG-based brain–computer interfaces," *J. Neural Eng.*, vol. 4, no. 2, pp. R1–R13, Jan. 2007, doi: 10.1088/1741-2560/4/2/r01.

[28] H. Kaur, H. S. Pannu, and A. K. Malhi, "A systematic review on imbalanced data challenges in machine learning: Applications and solutions," *ACM Comput. Surv.*, vol. 52, no. 4, pp. 1–36, Jul. 2020.

[29] S. Mallat and W. L. Hwang, "Singularity detection and processing with wavelets," *IEEE Trans. Inf. Theory*, vol. 38, no. 2, pp. 617–643, Mar. 1992.

[30] Y. LeCun *et al.*, "Backpropagation applied to handwritten zip code recognition," *Neural Comput.*, vol. 1, no. 4, pp. 541–551, 1989.

[31] R. M. Dudley, *Uniform Central Limit Theorems*. Cambridge, U.K.: Cambridge Univ. Press, 2014, vol. 142.

[32] B. Blankertz, R. Tomioka, S. Lemm, M. Kawanabe, and K. R. Müller, "Optimizing spatial filters for robust EEG single-trial analysis," *IEEE Signal Process. Mag.*, vol. 25, no. 1, pp. 41–56, Jan. 2008.

[33] P. L. Nunez *et al.*, "EEG coherency: I: Statistics, reference electrode, volume conduction, Laplacians, cortical imaging, and interpretation at multiple scales," *Electroencephalogr. Clin. Neurophysiol.*, vol. 103, no. 5, pp. 499–515, 1997.

[34] M. Miao, A. Wang, and F. Liu, "A spatial-frequency-temporal optimized feature sparse representation-based classification method for motor imagery EEG pattern recognition," *Med. Biol. Eng. Comput.*, vol. 55, no. 9, pp. 1589–1603, Sep. 2017.

[35] S. Kumar and A. Sharma, "A new parameter tuning approach for enhanced motor imagery EEG signal classification," *Med. Biol. Eng. Comput.*, vol. 56, no. 10, pp. 1861–1874, Oct. 2018.

[36] G. Liu, "It may be time to improve the neuron of artificial neural network," *TechRxiv*, Jun. 2020, doi: 10.36227/techrxiv.12477266.

[37] G. Pfurtscheller, C. Neuper, D. Flotzinger, and M. Pregenzerb, "EEG-based discrimination between imagination of right and left hand movement," *Electroencephalogr. Clin. Neurophysiol.*, vol. 103, no. 6, pp. 642–651, Dec. 1997.

[38] A. Gidon *et al.*, "Dendritic action potentials and computation in human layer 2/3 cortical neurons," *Science*, vol. 367, no. 6473, pp. 83–87, Jan. 2020.

[39] K. He, X. Zhang, S. Ren, and J. Sun, "Deep residual learning for image recognition," in *Proc. IEEE Conf. Comput. Vis. Pattern Recognit.*, Jun. 2016, pp. 770–778.

[40] H. Cho, M. Ahn, S. Ahn, M. Kwon, and S. C. Jun, "EEG datasets for motor imagery brain–computer interface," *GigaScience*, vol. 6, no. 7, p. 34, Jul. 2017.

[41] H. Cho, M. Ahn, S. Ahn, M. Kwon, and S. C. Jun, "Supporting data for 'EEG datasets for motor imagery brain computer interface' GigaScience database," 2017, doi: 10.5524/100295.

[42] M. Xia, J. Wang, and Y. He, "BrainNet viewer: A network visualization tool for human brain connectomics," *PLoS ONE*, vol. 8, no. 7, Jul. 2013, Art. no. e68910.

[43] K. Wang, M. Xu, Y. Wang, S. Zhang, L. Chen, and D. Ming, "Enhance decoding of pre-movement EEG patterns for brain–computer interfaces," *J. Neural Eng.*, vol. 17, no. 1, Jan. 2020, Art. no. 016033.

[44] G. Pfurtscheller and F. H. L. da Silva, "Event-related EEG/MEG synchronization and desynchronization: Basic principles," *Clin. Neurophysiol.*, vol. 110, no. 11, pp. 1842–1857, 1999.

[45] X. Zhao, J. Zhao, C. Liu, and W. Cai, "Deep neural network with joint distribution matching for cross-subject motor imagery brain-computer interfaces," *BioMed Res. Int.*, vol. 2020, pp. 1–15, Feb. 2020.

[46] B. Wahlberg, "System identification using Kautz models," *IEEE Trans. Autom. Control*, vol. 39, no. 6, pp. 1276–1282, Jun. 1994.

[47] J. R. Smith, F. Fatehi, C. S. Woods, J. F. Hauer, and D. J. Trudnowski, "Transfer function identification in power system applications," *IEEE Trans. Power Syst.*, vol. 8, no. 3, pp. 1282–1290, Aug. 1993.

[48] K. K. Krishnan and K. P. Soman, "CNN based classification of motor imaginary using variational mode decomposed EEG-spectrum image," *Biomed. Eng. Lett.*, vol. 1, no. 1, pp. 235–247, 2021, doi: 10.1007/s13534-021-00190-z.

[49] Y. He *et al.*, "Impaired small-world efficiency in structural cortical networks in multiple sclerosis associated with white matter lesion load," *Brain*, vol. 132, pp. 3366–3379, Dec. 2009.

[50] F. Lotte, M. Congedo, A. Lécuyer, F. Lamarche, and B. Arnaldi, "A review of classification algorithms for eeg-based brain–computer interfaces," *J. neural Eng.*, vol. 4, no. 2, p. R1, 2007.

[51] U. Chaudhary, N. Birbaumer, and A. Ramos-Murguialday, "Brain–computer interfaces for communication and rehabilitation," *Nature Rev. Neurol.*, vol. 12, p. 513, Aug. 2016.

[52] R. T. Schirrmeister *et al.*, "Deep learning with convolutional neural networks for EEG decoding and visualization," *Hum. Brain Mapping*, vol. 38, pp. 5391–5420, Nov. 2017.

[53] M. S. A. Graziano, "Ethological action maps: A paradigm shift for the motor cortex," *Trends Cognit. Sci.*, vol. 20, no. 2, pp. 121–132, Feb. 2016.